Interaction between Engineered Pluronic Silica Nanoparticles and Bacterial Biofilms: Elucidating the Role of Nanoparticle Surface Chemistry and EPS Matrix

Interaction between Engineered Pluronic Silica Nanoparticles and Bacterial Biofilms: Elucidating the Role of Nanoparticle Surface Chemistry and EPS Matrix

Stefania Vitale*, Enrico Rampazzo, Dishon Hiebner, Henry Devlin, Laura Quinn, Luca Prodi, and Eoin Casey

***ACS Appl. Mater. Interfaces* 2022, 14, 30, 34502–34512**

The final published version is available online at:
https://doi.org/10.1021/acsami.2c10347

Interaction between engineered Pluronic silica nanoparticles and bacterial biofilms: elucidating the role of nanoparticle surface chemistry and EPS matrix

Stefania Vitale[1]†*, *Enrico Rampazzo*,[2] *Dishon Hiebner*,[1§] *Henry Devlin*,[1] *Laura Quinn*,[1] *Luca Prodi*,[2] *Eoin Casey*[1]

[1] UCD School of Chemical and Bioprocess Engineering, University College Dublin, Dublin 4, Ireland.

[2] Dipartimento di Chimica "Giacomo Ciamician", Università degli Studi di Bologna, Via Selmi 2, 40126 Bologna, Italy.

† Current address: Université de Strasbourg, CNRS, ISIS, 8 allée Gaspard Monge, 67000 Strasbourg, France.

§ Current address: School of Pharmacy and Biomolecular Sciences, Irish Centre for Vascular Biology, Royal College of Surgeons in Ireland, Dublin 2, Ireland.

*Corresponding author

svitale@unistra.fr

KEYWORDS: fluorescent silica nanoparticles, bacterial biofilm, bio-nano interaction, surface chemistry, *Pseudomonas Putida*

ABSTRACT

Nanoparticles (NPs) are considered a promising tool in the context of biofilm control. Many studies have shown that different types of NPs can interfere with the bacterial metabolism and cellular membranes, thus making them potential antibacterial agents; however fundamental understanding is still lacking on the exact mechanisms involved in these actions. The development of nanoparticle-based approaches for effective biofilm control also requires a thorough understanding of how the chosen nanoparticles will interact with the biofilm itself, and in particular with the biofilm self-produced extracellular polymeric matrix (EPS).

This work aims to provide advances in the understanding of the interaction between engineered fluorescent pluronic silica (PluS) nanoparticles and bacterial biofilms, with a main focus on the role of the EPS matrix in the accumulation and diffusion of the particles in the biofilm. It is demonstrated that the particle surface chemistry has a key role in the different lateral distribution and specific affinity to the biofilm matrix components. The results presented in this paper contribute to our understanding of biofilm-nanoparticle interactions and promote the principle of rational design of smart nanoparticles as an important tool for anti-biofilm technology.

INTRODUCTION

Bacterial biofilm formation is a phenomenon that has a significant impact in our everyday lives, from infectious diseases to performance losses in the process industries due to biofouling. Bacterial biofilms are dynamic, structurally complex, integrated multi-cellular communities of surface-adhering microorganisms that are embedded in an extracellular polymeric matrix (EPS).[1] The EPS is made up of a mixture of components including polysaccharides, proteins, nucleic acids and lipids and plays an important role in maintaining the integrity of the biofilm, from both a physiological and mechanical point of view.[2]

Given the emergence of multidrug resistant bacterial strains, which has severely decreased the efficacy of antibiotic treatments,[3] the need for new strategies for biofilm prevention and disruption is

continuously increasing. Recently, the potential to exploit nanoparticles (NPs) for biofilm control and eradication has been a growing interest among the scientific community.[4]

Different families of nanomaterials and NPs have been considered as promising antimicrobial and antibiofilm agents, and evidence of antibacterial effects has already been demonstrated for various chemical compositions (Ag, ZnO, Au, chitosan), surface modification[5] and morphology.[6] While many studies in the literature point out that NPs showing antibacterial action most likely interfere with bacterial metabolism and cellular membranes,[3] what is not yet fully understood is the role of the EPS in the general framework of NPs-biofilm interaction.

Being a physical barrier that embeds and shields the bacterial cells, the EPS matrix largely influences the uptake and reduces the mobility of external agents within the biofilm, including small molecules (*e.g.* antibiotics) and nanomaterials.[7] Recent research reveals that the matrix effectively acts as a molecular sieve, hindering the penetration of substances that are larger than its pore size; furthermore, such diffusional-barrier activity has also been correlated to the structural density of the polysaccharides backbone, the microcolonies distribution, the specific matrix chemical composition, the presence of gradients in the concentration of biomolecules and other physiological parameters (e.g. temperature and pH).[8] The diffusion of molecules within the matrix has been observed and extensively investigated in the context of improving antibiotic therapies and disinfection protocols, and different analytical methods have been developed to assess mass transport and diffusion coefficients within the EPS matrix.[9] More recently the same tools have been optimised to study the dynamics of NP uptake and mobility in bacterial biofilms. The EPS strongly affects the extent of nanoparticle capture, penetration and diffusion within the biofilm.[10] These three variables are fundamental for the design of efficient nanoparticle-based systems for biofilm control: the particles must be able to effectively penetrate and diffuse throughout the biofilm thickness to reach their target (bacterial cells, EPS matrix or both).

In this paper we studied the interaction between engineered fluorescent pluronic silica (PluS) NPs and bacterial biofilms, with the aim of advancing our understanding on the role of the EPS matrix in

such interactions. The matrix influence on the particles diffusion and distribution within the biofilm was thoroughly investigated both in *in vivo* biofilms and in *in vitro* studies. Engineered fluorescent PluS particles have already shown promise in the context of biomedical applications, such as tissue and cell labelling and imaging (both *in vivo* and *ex vivo*), as well as environmental applications, such as heavy-metal sensing.[11] For our investigation, biofilms of the strain *Pseudomonas putida* (*P. putida)* were chosen as the model microorganism. Gram-negative *P. putida* bacteria are ubiquitous in the natural environment[12] and prevalent in industrial settings. They produce biomolecule-rich biofilms,[13] which have been reported to negatively affect industrial water treatment systems and act as reservoir for antibiotic resistance determinants in hospital environments.[12, 14]

EXPERIMENTAL SECTION

- Materials

Pluronic F127, tetraethyl orthosilicate (TEOS, 99.99%), chlorotrimethylsilane (TMSCl, ≥ 98%), acetic acid (HOAc, ≥ 99.7%), HCl (≥37%), sodium alginate, bovine serum albumin (BSA), calcium chloride ($CaCl_2$), ethanol (EtOH), glycerol, King B agar, magnesium sulfate ($MgSO_4$), Mowiol 4-88 and phosphate buffered saline (PBS) and dichloromethane were purchased from Sigma-Aldrich. Carboxyethylsilanetriol sodium salt (25% w/w water solution, CETS) was purchased from GELEST. Potassium phosphate dibasic was purchased from Honeywell, Fluka™.

Rhodamine B triethoxysilane derivative (RhB-TES) was synthesized as previously reported.[15]

Sypro® Orange and Syto™ 9 were purchased from ThermoFischer Scientific. Fluorescein (FITC)-labelled Lectin Kit I was purchased from Vector Laboratories.

Clear 96-well plates were purchased from SARSTEDT. Costar® Black 96-well plates were purchased from Corning.

UF tubes (Amicon Ultra-0.5 mL, cutoff 100 KDa) were purchased from Millipore. Dialysis was performed versus water at room temperature under gentle stirring with regenerated cellulose dialysis tubing (Sigma, mol wt cutoff >12 kDa, av diameter 33 mm).

Grade 1 pure water (18.2 MΩ cm^{-1}), was obtained from an Elga Process Water System (Biopure 15 and Pureflex 2, Veolia).

- Nanoparticles synthesis

Core–shell silica-PEG (poly(ethylene glycol)) NPs bearing carboxylic groups on the PEG surface (PluS-PEG-COOH) and core–shell silica-PEG NPs with a carboxyl-functionalised silica core (PluS-PEG) were synthesized adapting previously reported procedures.[11d, 11e, 16] The reagents and their quantities used for each synthesis are listed in Table 1, and a schematic of the synthetic procedure is presented in Figure 1.

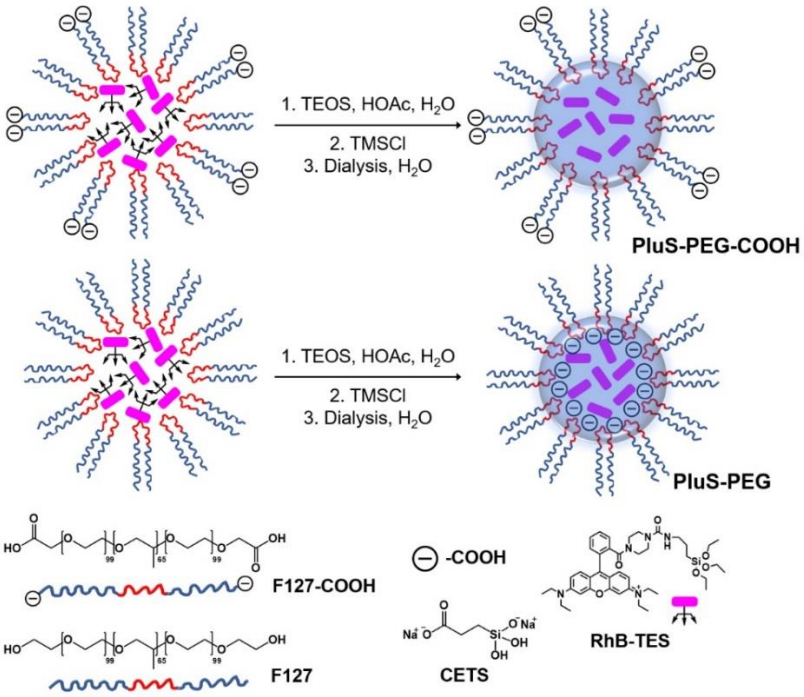

Figure 1. Scheme of the PluS particles synthesis.

Table 1. Reagents used for the synthesis of PluS nanoparticles.

NP sample	F127 mg (mmol)	F127-COOH mg (mmol)	RhB-TES mg (mmol)	Acetic acid, 1.00 mol L^{-1}, µL	TEOS µL (mmol)	CETS µL (mmol)	TMSCl µL (mmol)
PluS-PEG	100	--	1.34 ($1.57x10^{-3}$)	1535	175 (0.78)	12, (0.018)	10 (0.079)
PluS-PEG-COOH	70	30	1.34 ($1.57x10^{-3}$)	1535	175 (0.78)	--	10 (0.079)

In a typical preparation, Pluronic F127 and RhB-TES dye were initially solubilized with 1–2 mL of dichloromethane in a 20 mL glass scintillation vial, and the solvent was evaporated from the resulting solution under vacuum at room temperature. NaCl (67 mg) was added to the solid residue, and the mixture was solubilized at 25°C under magnetic stirring with 1535 µL of 1.0 M acetic acid. TEOS (175 µL, 0.78 mmol) was then added to the resulting aqueous homogeneous solutions.

For the preparation of PluS-PEG-COOH particles, TMSCl (10 µL, 0.079 mmol) was added to the reaction mixture after 3 hours, and the mixture was kept under stirring conditions for 20 h at 25°C before dialysis treatments. For the preparation of PluS-PEG particles, TEOS addition was followed by CETS addition and the mixture was kept under stirring for 12 hours; after this time TMSCl (10 µL, 0.079 mmol) was added, and the mixture was kept under stirring for further 20 h at 25°C before dialysis treatments.

The dialysis purification steps were carried out against Milli-Q water on a precise amount of nanoparticle solution (1500 µL, RC membrane cut-off 12 kDa, 20 hours). The dialyzed dispersion of

nanoparticles was diluted to a final volume of 5000 µL, resulting in a stock solution at 20 µM concentration, as reported elsewhere.[15]

Working solutions of PluS-PEG and PluS-PEG-COOH were prepared through dilution of the stock solutions with water to a final concentration of 200 nM.

Absorption and fluorescence spectra were acquired at 25°C for both particles solutions (SpectraMax iD3, Molecular devices). NPs were characterised through dynamic light scattering (DLS) and Zeta potential measurements (Zetasizer Nano ZS, Malvern Instruments); PluS-PEG and PluS-PEG-COOH aqueous dispersions at working concentration (200 nM) were analysed in a folded capillary cell. For size measurements, experiments were run in triplicate, with 10 runs for each measurement. For zeta potential measurements, all experiments were run three or five times, with 15 scans for each run.

- Bacterial Culture

Pseudomonas putida strains (*P. putida*) were used in this study, either engineered GFP-expressing PCL 1482 or wild type PCL 1455. Bacterial cultures were stored at –80°C in 25% glycerol (w/v). For biofilm cultivation, thawed aliquots were streaked onto King B agar plates, supplemented with tetracycline (40 µg mL^{-1}), and incubated for 24 hours at 30°C. A single bacterial colony was used to inoculate 50 mL of sterile King B medium in a 250 mL Erlenmeyer flask and incubated at 30°C with shaking at 200 RPM overnight (16 – 18 hours) to an approximate optical density at 600 nm (OD_{600}) between 2.3 – 2.6 (the medium was supplemented with tetracycline (40 µg mL^{-1}) when culturing *P. putida* PCL 1482). The overnight cultures were then diluted with fresh sterile King B medium to a final OD_{600} of 1.

For confocal laser scanning microscopy (CLSM) measurements and EPS extraction, biofilms were grown on glass coverslips, following a procedure adapted from Safari *et al*.[17] The glass coverslips (24 mm X 50 mm) were inserted vertically in sterile 50 mL centrifuge tubes and 5 mL were added of diluted culture (OD_{600} 1) supplemented with $CaCl_2$ to a final concentration of 1.5 mM. The tubes

were plugged with sterile cotton wool and then incubated for 72 hours at 30°C with shaking at 100 RPM. The medium was not refreshed throughout the incubation period.

For the assessment of the NPs entrapment in the biofilms, *P. putida* PCL1482 biofilms were cultivated in black 96-well plates, to reduce the background signal when measuring fluorescence intensity, following a previously reported procedure.[18] Firstly a bacterial culture mix was prepared with tetracycline (40 µg mL^{-1}), calcium chloride (1.5 mM), magnesium sulfate (1.5 mM) and the bacterial culture (OD_{600} 1); 150 µL of this mixture was then added to each well and the plate was then covered with a gas-permeable rayon membrane, to allow aeration. Biofilm formation was then carried out at 28°C with shaking at 125 rpm for 24 hours. Following biofilm formation in 96-well plates, the cultures were washed three times with sterile water to remove planktonic cells and residual spent media from the wells.

- CLSM and colocalisation analysis

Before analyses, biofilm-coated coverslips were carefully removed from centrifuge tubes and gently washed three times with sterile water to remove loosely attached cells. For both qualitative and quantitative imaging, biofilms were sequentially labelled with two fluorescent dyes as follows: (I) Concanavalin A (ConA) conjugated to FITC, which labels polysaccharides in the biofilm matrix by binding to mannose and glucose residues, 20 µg mL^{-1}; (II) Sypro® Orange (1 in 5000 dilution), which labels most EPS proteins. For staining, coverslips were placed horizontally on a sample holder and 150 µL of each fluorescent probe solution was drop casted onto the biofilm, followed by incubation in the dark for 15 minutes. After incubation, the biofilms were gently rinsed three times with water to remove unbound stains. This was repeated for each probe. Subsequent to fluorescent probe staining of the biofilm components, 150 µL of each NPs solution (200 nM) was drop casted on top of the biofilm. Unstained samples with or without exposure to nanoparticle solutions were used as controls. Tris-buffered Mowiol 4-88 mounting medium was used to mount each coverslip onto a glass microscope slide (25 mm x 75 mm x 1mm) as previously reported.[19] The mounted slides were allowed

to dry for at least 1 hour at room temperature in the dark. Horizontal plane z-stack images were acquired with an Olympus FluorView FV1000 CLSM attached to an inverted Olympus IX81 microscope with a 60x/1.35 NA UPL SAPO oil immersion objective (Olympus Optical, Tokyo, Japan). The microscope was equipped with 405 nm, 488 nm, 543 nm and 633 nm laser lines. All images were acquired equally: 1x digital zoom, a scanning speed of 2.0 μs/pixel, with 2x Kalman line averaging and sequential channel acquisition. At least three image stacks, with a z-step of 1μm, from each of three independent experiments were acquired and analysed using Fiji image processing software.[20] Images were background subtracted and median filtered (0.5 pixel radius) and colocalisation analysis were performed using the "JaCoP" plugin.[21] Mander's correlation coefficients were used for reporting colocalisation between PluS particles and EPS matrix macromolecules and therefore the colocalisation ratios were independent of signal intensity and overall abundance of fluorescence signal.

To quantify the penetration of the NPs into the biofilm, normalized fluorescence signals from the red channel observed in orthogonal xz and yz views from z-stack confocal imaging were utilized. Experiments were performed in triplicate, and only representative images are shown.

- Entrapment experiments

The entrapment of PluS particles in the biofilms was assessed using a previously reported method.[18] Briefly, 150 μL of the aqueous particles suspension (200 nM concentration) was added to each well of the 96-well plate where biofilms were grown. Fluorescence intensity from both the biofilm-exposed particles and the control sample (150 μL of 200 nM particles solution in water) was measured every 10 minutes under shaking conditions using a plate reader (SpectraMax iD3, Molecular devices), with the first reading taking place one minute after initial exposure. The entrapment of the particles in the biofilm was calculated for each well using the following equation:

$$NP\ entrapment = \frac{I_C - I_N}{I_C} \times 100$$

where I_c is the fluorescent intensity of the control sample and I_N is the fluorescent intensity of the biofilm-exposed particles. By measuring the reduction in fluorescence intensity between solutions of nanoparticles exposed to the biofilms and the control particles solution, the overall entrapment of particles in the biofilm samples can be calculated, independently of particles size or concentration. Four independent experimental replicates were carried out for each particle sample, with 24 biological replicates in each run.

- Stability measurements *via* Zeta potential and DLS analysis of PluS-EPS solutions

For these experiments, PluS NPs were exposed to solutions of extracted EPS, in order to assess *in vitro* the interaction between the particles and the matrix, and to find a relationship with the data obtained from entrapment measurements and confocal imaging.

EPS was extracted from 72 hours biofilms grown on glass coverslips, using a procedure based on cation-exchange resin (CER) extraction adapted from Jachlewski *et al*.[22] Briefly, the biofilms were scraped from the glass coverslips, gently washed with PBS buffer and then resuspended in 0.5 mL of a NaCl 0.9% (w/v) solution. After sonication for 2 minutes, the cation exchange Dowex® resin was added (1% w/v) and the EPS extracts were shaken at 300 RPM for 2 hours at 4°C in the dark. An EPS solution was obtained from the supernatant centrifugation (20,000 g for 20 minutes at 4°C) and filtration (Millipore® 0.22 µm pore membrane filter). The obtained EPS extracts were stored at -80°C until their use.

For PluS-PEG and PluS-PEG-COOH solutions in water the final concentration (used for sample analysis) was of 200 nM for all the measurements, consistently with environmentally-relevant concentrations.[23] For the stability experiments, unbuffered aqueous dispersions were used in order to

ensure that no interactions or particle surface modification were accidentally induced before the exposure to biomolecules.

The particles solutions were exposed to extracted EPS solutions at concentrations ranging from 100.0 to 0.5 μg mL^{-1}. The concentration range was extrapolated from EPS matrix quantification after extraction, to be representative of the actual EPS concentration in the biofilm.

After 30 minutes of incubation, the PluS-EPS complexes were analysed by DLS and Zeta potential measurement, in the same instrument and experimental conditions previously described for nanoparticles characterisation.

In order to identify the contributions of polysaccharides and proteins, PluS particles were also exposed to solutions of sodium alginate (5.000 to 0.025 μg mL^{-1}) and BSA (10.00 to 0.05 μg mL^{-1}), and DLS and zeta potential analysis were carried out in the same experimental conditions already described for the characterisation of the dispersions of NPs alone. Alginate and BSA were chosen as model polysaccharide and protein, respectively; the concentrations used are representative of the concentrations of proteins and carbohydrates in the matrix, which were quantified on the EPS extracts through Lowry and phenol-sulphuric acid assays, respectively.

EPS, BSA and alginate solutions were all prepared in NaCl 0.9% (0.15 M), and the same NaCl concentration was maintained for the samples by adding appropriate volumes of a 5% NaCl stock solution. All the NP-biomolecules test solutions were analysed immediately after the incubation period without any purification procedure, consistent with an *in vitro* assessment of the colloidal stability.

- Statistical analysis

One-way analysis of variance (ANOVA) was used to evaluate statistical significance ($p < 0.05$). Error bars represent standard error of the mean, extrapolated on at least three separate experiments.

RESULTS AND DISCUSSION

- NPs characterisation

PluS-PEG and PluS-PEG-COOH NPs present a core-shell structure, featuring a silica core and an outer shell of PEG. The particles differ in the position of the carboxylic groups in the core shell-structure, localised on the silica core for PluS-PEG and on the PEG shell for PluS-PEG-COOH, respectively. The carboxylic groups are also responsible for the negative charge of the particles; depending on the group position, the charge will be either exposed on the outer PEG shell or buried beneath the polymeric layer. The two particles have the same core size (≅ 10 nm) and similar hydrodynamic diameter, as measured by, respectively, TEM (Figures S1-S2) and DLS (Table 2, Figures S3-S4). The difference in particle size obtained with the two techniques is expected, and it is due to the different physical variables measured (i.e. hydrodynamic diameter dH of the NP in solution for DLS, which accounts also for the solvation sphere surrounding the particles, and diameter of the dry particles for TEM, always smaller than dH).[24]

It is well established that surface functionality and properties of nanomaterials dictate their behaviour in biological media, including bacterial biofilms.[25] As the two PluS particles have similar structure, composition and size, it is expected that any difference in the way they behave once in contact with the biofilm and its components is caused by the different position of the carboxylic group on the particle surface.

Table 2. DLS and Zeta potential measurements for 200 nM aqueous dispersions of PluS-PEG and PluS-PEG-COOH NPs.

Sample	**d_H (nm)**	**PDI**	**Zeta potential (mV)**
PluS-PEG	45 ± 1	0.20	-16 (±1)
PluS-PEG-COOH	36 ± 3	0.38	-8 (±2)

d_H: hydrodynamic diameter; PDI: polydispersity index.

- Distribution and penetration into the biofilm

Initial investigations focussed on the ability of the particles to penetrate into the biofilm and analysis of their distribution (both in the lateral and axial directions within the biofilm thickness). These variables are key to many applications, such as effective nanoparticle-based drug-delivery and biofilm dispersing agents.[26]

In Figure 2 the entrapment results are shown for both PluS-PEG and PluS-PEG-COOH. In absolute percentage of captured particles, PluS-PEG show a greater entrapment percentage by the biofilm compared to PluS-PEG-COOH, by 25% and 12%, respectively. The time profiles show slight differences: the entrapment of PluS-PEG particles by the biofilm increases until a plateau is reached, whereas for PluS-PEG-COOH the trend indicates an initial increase in the uptake, quickly followed by a slight decrease and then stabilisation.

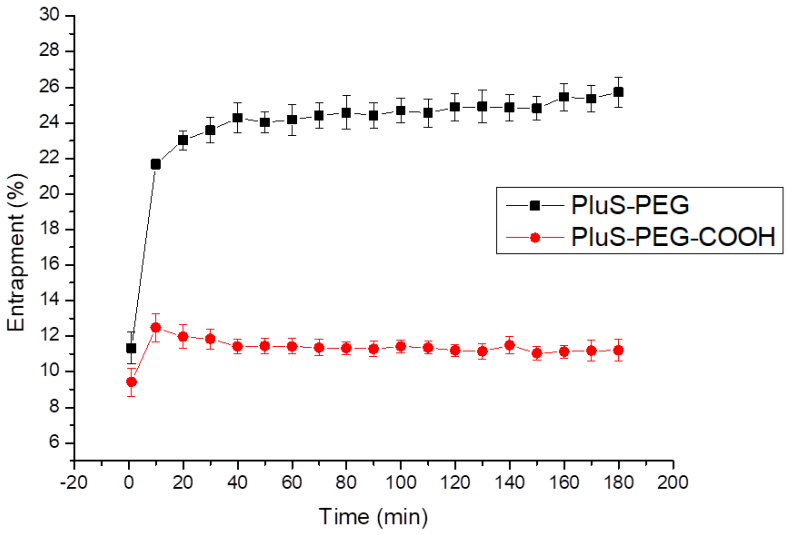

Figure 2. NPs entrapment profiles for aqueous dispersions of PluS-PEG (200 nM) and PluS-PEG-COOH (200 nM). Error bars represent standard error of the mean (n = 4). Statistical differences were assessed by one-way ANOVA ($p < 0.05$).

In Figure 3 confocal images and orthogonal xz and yz views are presented for *P. putida* exposed to PluS-PEG and PluS-PEG-COOH aqueous dispersions (200 nM). Both sets of particles can be observed as penetrating through the entire thickness of the biofilm, as shown in the orthogonal projections. Penetration inside the microcolonies is observed, with a higher concentration of particles in the biofilm inner core (white arrows). Such accumulation of NPs within the biofilm is often observed and can be explained with a diffusion-driven penetration of the nanoparticles within the matrix.[27] The particle accumulation in the inner core is more pronounced for PluS-PEG-COOH, as it can be concluded from the penetration profiles (Figure 3c)): the sigmoidal curve for Plus-PEG-COOH is correlated to a higher percentage of particles distributed towards the inner portions of the biofilm, showing preference for the inner core of the microcolonies (seen as yellow in Figure 3b)) while the linear profile for Plus-PEG shows a more even distribution throughout the entirety of the biomass.

With regards to the particle lateral distribution, important differences are observed (

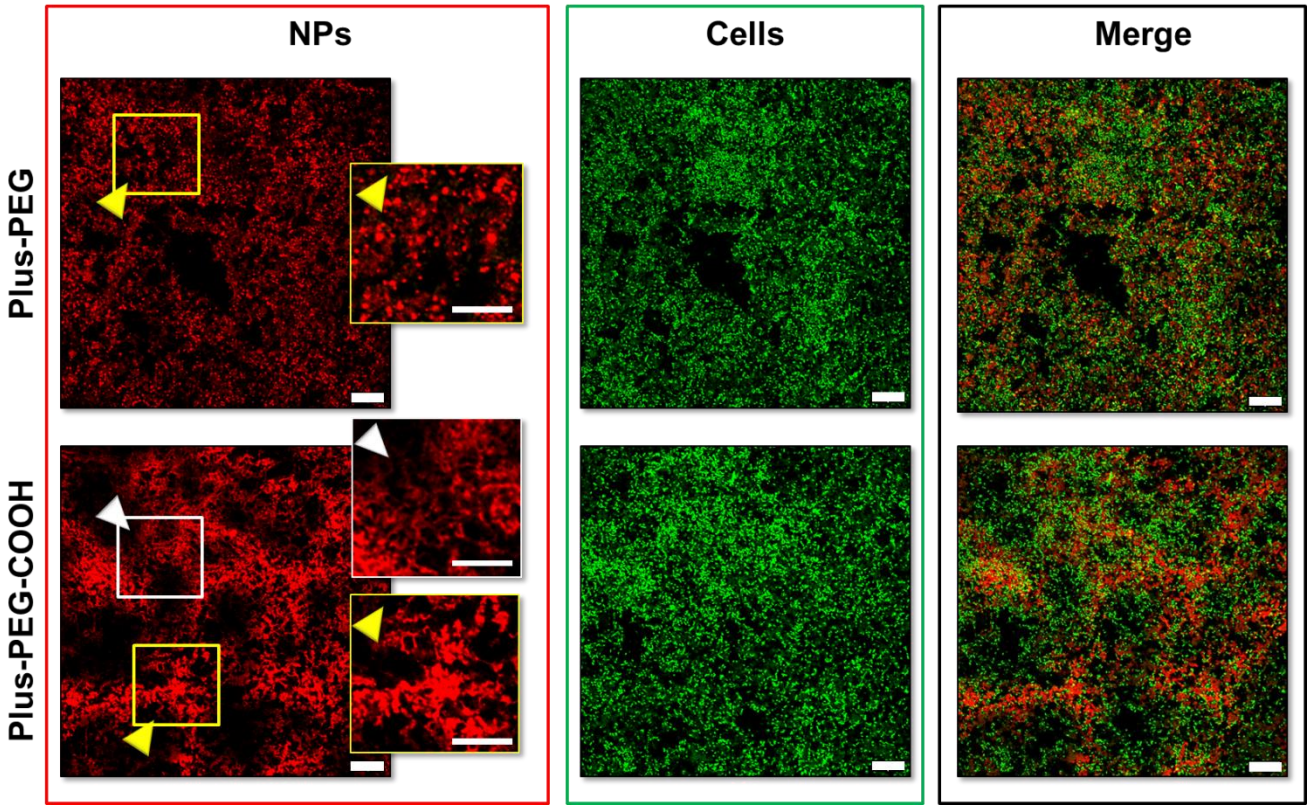

Figure ***4***).

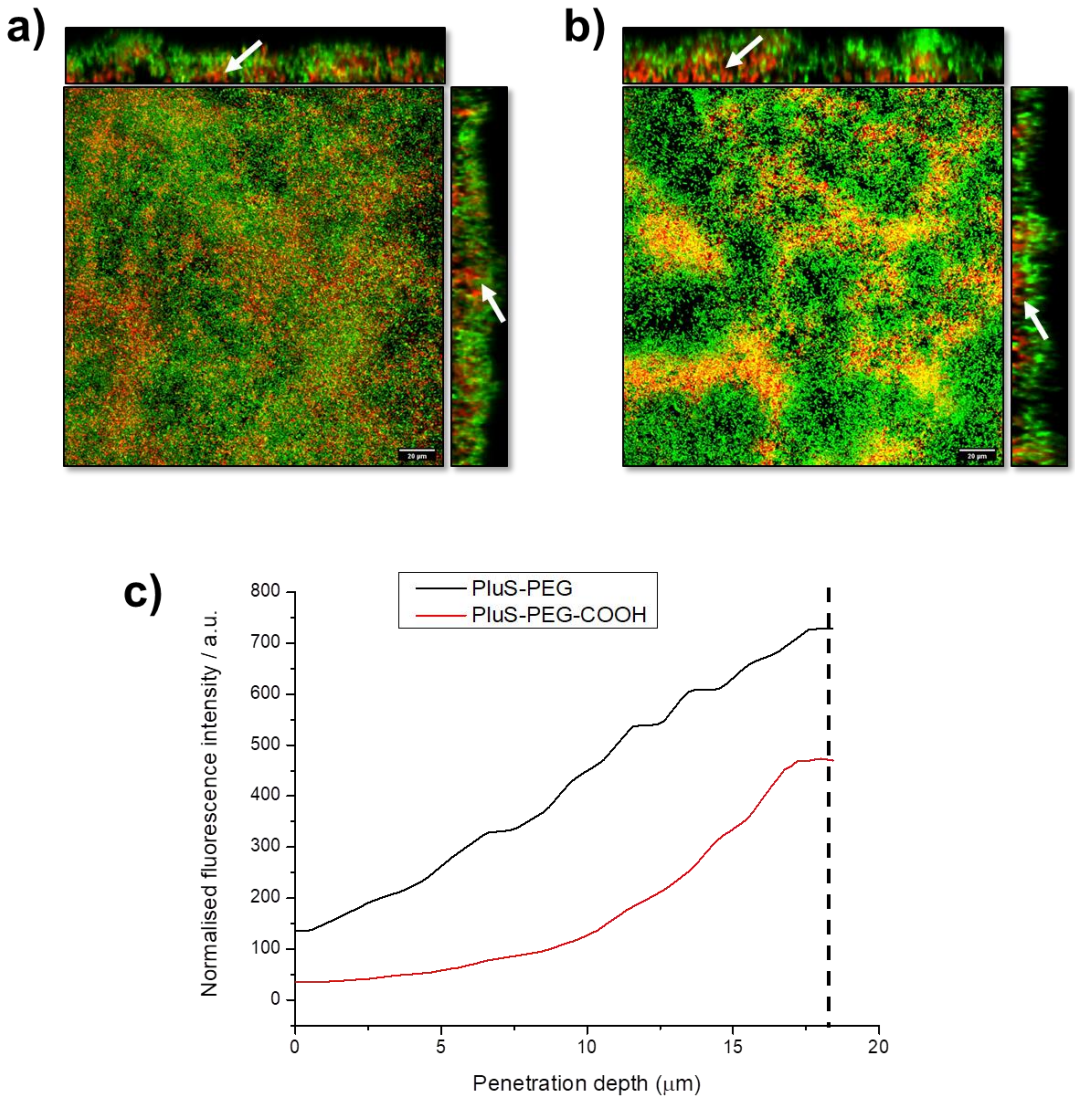

Figure 3. Confocal z-stack images with xz and yz orthogonal views of *P. putida* PCL 1482 exposed to a) PluS-PEG and b) PluS-PEG-COOH dispersions (white arrows indicate biofilm inner core, scale bars are 20 μm); c) penetration profiles of PluS-PEG and PluS-PEG-COOH into *P. putida* biofilms (the x-axis shows penetration depth, where 0 μm represents the top layer of biofilm and ~18.4 μm (represented by dashed vertical line) represents the bottom layer of biofilm; the y-axis shows the normalised fluorescence intensity of red channels).

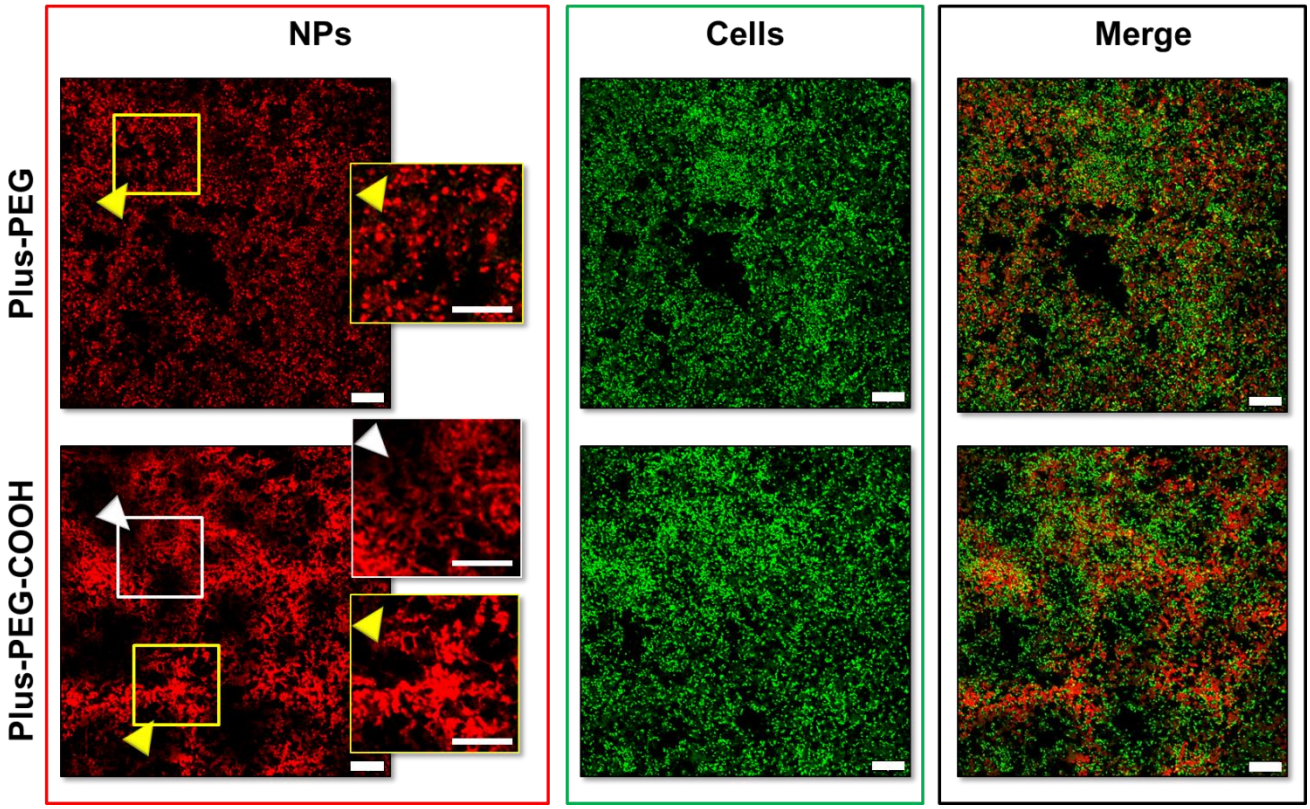

Figure 4. Single slice confocal images of *P. putida* PCL 1482 exposed to Plus-PEG (top) and PluS-PEG-COOH (bottom) particles dispersions. Images are taken in the same position on the biofilm sample. Arrowheads indicate particular nanoparticle distribution features, which are emphasised in the high-magnification insets. Scale bars are 20 µm, except for the high-magnification insets where they are 5 µm.

For PluS-PEG the binding pattern results mostly in an even lateral distribution throughout the EPS matrix between cells (white arrowheads), but also very well-defined circular agglomerates of ~ 1 µm size are observed (yellow arrowheads and high-magnification detail). For PluS-PEG-COOH the binding pattern shown is either string-like network (white arrowheads and related inset) or agglomeration in clumps (yellow arrowheads and related inset).

From the confocal image sections (Figure 3) it is clear that both nanoparticle types are able to effectively penetrate through the entire biofilm thickness. There is no evidence of accumulation of the particles on the outer surface of the biofilm. In general, it is understood that the nanoparticle penetration into the biofilm is largely determined by the particle size, with particles having diameter of less than 50 nm being able to readily diffuse within the matrix;[27] this size limit has been associated to the dimension of the water-filled channels (pores) of the matrix. The particles used in this work have comparable size, and in both cases smaller than 50 nm, therefore this justifies the similar penetration profile. However, the two particles exhibit a different lateral distribution (

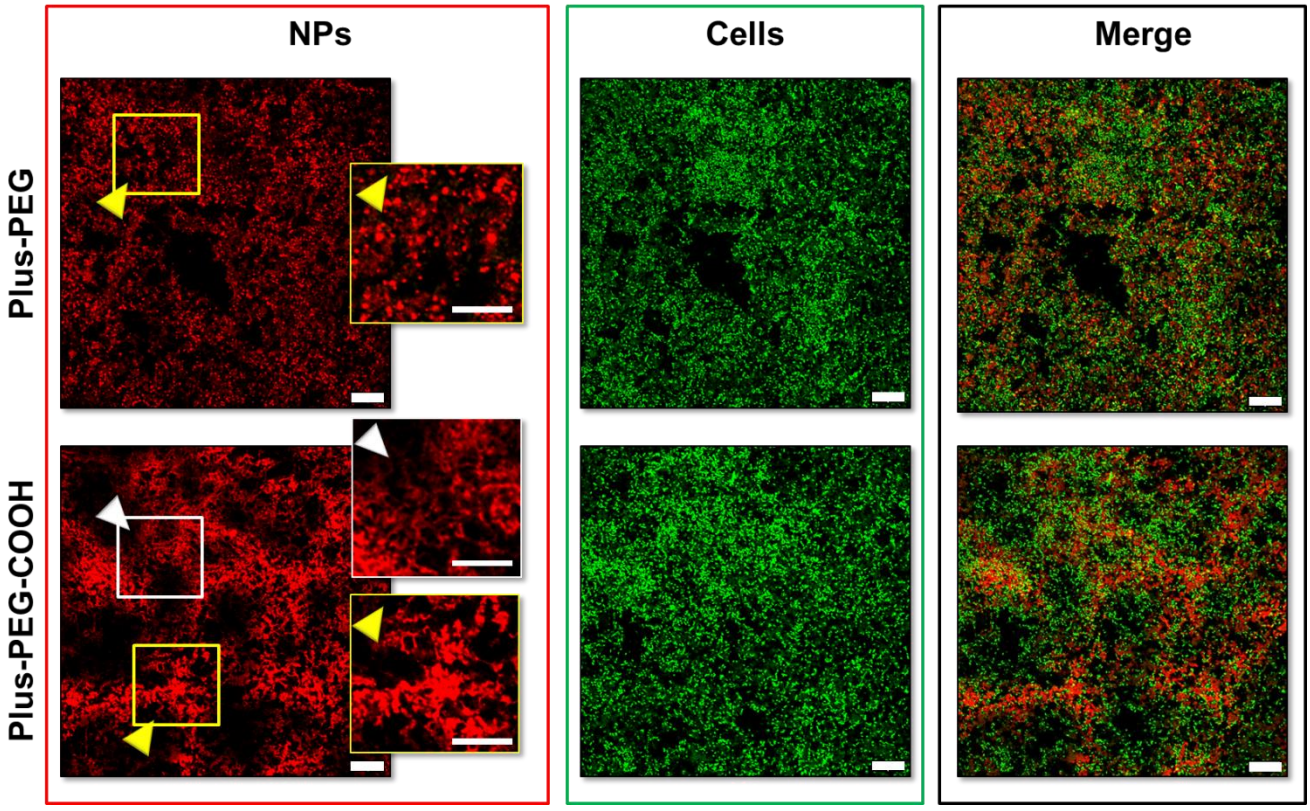

Figure ***4***): PluS-PEG are evenly distributed and some circular agglomerates can be observed uniformly spread, whereas PluS-PEG-COOH are localised in more specific areas following a string-like pattern. From these data it can be inferred that the particle distribution in the biofilm is driven by selective binding preferences with matrix components, seemingly non-specific for PluS-PEG (resulting in uniform distribution and aggregation) and more specific for PluS-PEG-COOH (well defined binding patterns). The spatial distribution of biomolecules in the matrix is known to be highly heterogeneous;[28] in addition, it has been already reported that specific binding affinities and

interactions with different EPS biomolecules can occur as a function of the surface chemistry and composition of the particles, to the extent that the NPs can be purposely tailored to exploit such interactions for specific biomolecules targeting.[5b, 25c, 29]

- Colocalisation of PluS NPs to EPS matrix proteins and polysaccharides

Colocalisation analysis was carried out to further investigate if specific binding affinities are occurring for the two particles with particular matrix components.[30] The analysis was carried out on confocal z-stack images of biofilm samples firstly stained with either Sypro Orange or ConA-FITC, and subsequently exposed to PluS particles dispersions; the two stains are specific for proteins and polysaccharides, respectively. Representative single slice confocal images of stained samples are presented in Figure S6 and Figure S7. By analysing the degree of nanoparticle-stain colocalisation, information can be extrapolated on specific binding affinities of the particles to biofilm components. The results are reported in Table 3. The terminology for describing colocalisation data classifies weak colocalisation ranging from 0 to 0.39, moderate colocalisation from 0.4 to 0.69, and strong colocalisation from 0.7 to 1.0.[31]

Both types of nanoparticle exhibit a moderate colocalisation to polysaccharides, with a ratio of 0.53 for PluS-PEG and 0.49 for PluS-PEG-COOH, respectively. A different trend is observed for the colocalisation to proteins, namely moderate for PluS-PEG (0.62 ratio) and strong for PluS-PEG-COOH (0.81 ratio).

Table 3. Colocalisation analysis of PluS NPs and EPS matrix proteins and polysaccharides.

Sample	**Polysaccharides**		**Proteins**	
	Colocalisation ratio (*)	SD	Colocalisation ratio (*)	SD
PluS-PEG	**0.53**	0.07	**0.62**	0.04

PluS-PEG-COOH	**0.49**	0.03	**0.81**	0.04

(*) Fiji's JaCoP colocalization analysis (Mander's correlation coefficients) was conducted to examine pixel to pixel correlation in separate channels over space in several z-stack CLSM images. Data are representative of three separate experiments, each of which contained at least three z-stack CLSM images.

According to these data both particles show moderate colocalisation to the polysaccharide components of the matrix; this finding is consistent with the axial distribution that both sets of PluS particles show through the biofilm depth, considering that the polysaccharide network is one of the main constituent of the biofilm matrix scaffold.[28a, 32] Interestingly, a different trend is shown for the colocalisation to proteins, namely moderate for PluS-PEG and high for PluS-PEG-COOH particles, respectively. In general, nanoparticle interaction with proteins is a spontaneous phenomenon that occurs whenever any nanoparticle enters into contact with a biological medium, and leads to the formation of a protein-corona on the particle surface.[33] The affinity of both PluS particles for proteins (moderate for PluS-PEG and strong for PluS-PEG-COOH) might be the consequence of this interaction. Our data are also consistent with previously published results, where a certain affinity for matrix proteins was observed for PEG and PEG-carboxy-functionalised cadmium selenide quantum dots within *P. aeruginosa* biofilms.[34]

In comparison to PluS-PEG, the more significant colocalisation of PluS-PEG-COOH to proteins can be ascribed to the interaction of the carboxylic groups, exposed on the particle shell, with amino acid residues on the matrix proteins; this type of particle-protein interaction has been reported for different carboxy-functionalised particles *via* electrostatic interaction and hydrogen bonding.[35] In contrast, in the case of PluS-PEG the carboxyl groups are buried under the PEG shell, so a potential interaction with EPS biomolecules is likely hindered by the polymeric layer, and this would be consistent with the lower colocalisation ratio to proteins calculated for PluS-PEG.

- Stability tests on PluS-EPS solutions

To further elucidate the mechanism involved in the interaction of the PluS particles with the EPS matrix and its components, stability experiments were carried out in solution, exposing the particles to aqueous solutions of the biofilm matrix. These experiments aimed to analyse the degree of colloidal stability of particles dispersions in aqueous solutions of model main components of the biofilm matrix (proteins and polysaccharides) as well as in solutions of EPS extracts; the resulting data can provide insights on the particles interaction with the biofilm matrix.[36] It should be pointed out that although *in vivo* biofilms are rather complex and heterogeneous systems, *in vitro* simplified models provide a useful tool in biofilm research for understanding fundamental questions and complement *in situ* studies.[37]

DLS size (hydrodynamic diameter, dH) and zeta potential measurements are presented in Figure 5 and Figure 6, respectively, for PluS-EPS, PluS-alginate and PluS-BSA samples. The concentration of the test solutions was normalised so that to that each measurement point is representative of the concentration of proteins (modelled with BSA) and polysaccharides (modelled with alginate) present for a specific concentration of EPS.

A general increase of the hydrodynamic ratio ($p < 0.05$) is reported for PluS-PEG at increasing concentrations of all the test solutions (Figure 5a)). This supports that particle aggregation is promoted by all the aqueous model solutions of the main components of the biofilm matrix.

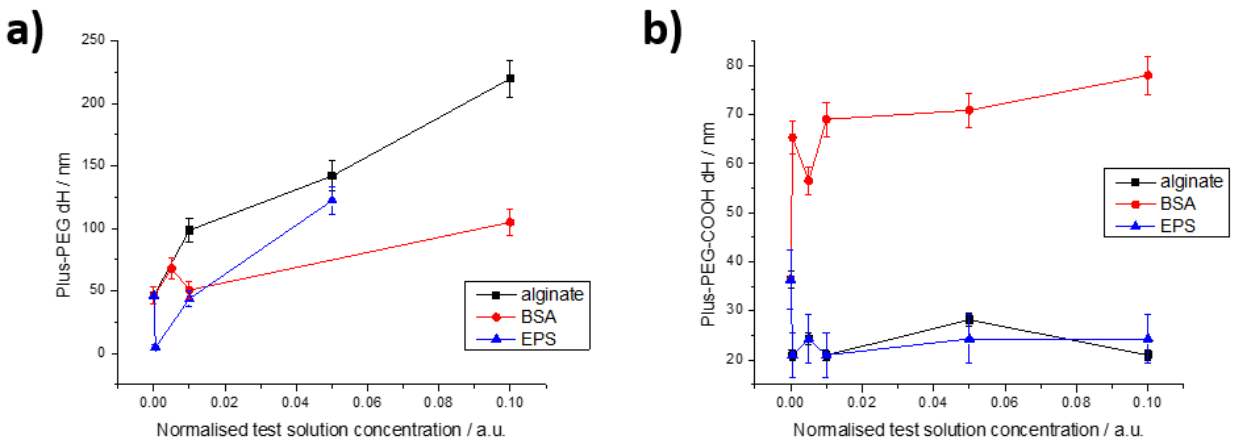

Figure 5. Hydrodynamic ratio measured by DLS for a) PluS-PEG and b) PluS-PEG-COOH dispersions exposed to *P. putida* EPS solutions. Error bars represent standard error of the mean (n = 3). Statistical differences were assessed by one-way ANOVA ($p < 0.05$).

A completely different pattern is observed for PluS-PEG-COOH particles (Figure 5b)). The exposure to EPS extract seems to decrease the partial interaction between PluS-PEG-COOH NPs, with a sharp hydrodynamic size decreases to a value of 25 nm, which remains constant with further increase in the concentration of the matrix solution ($p > 0.05$). The same trend is observed for the NP-alginate samples. In the case of NP-BSA samples the size increases to a constant value of 70 nm, independent of the protein concentration, with the only exception being the sample containing 0.1 ug/mL of BSA ($p < 0.05$). On the whole, for PluS-PEG-COOH no aggregation is observed.

With respect to the zeta potential measurements, for both particles there is no significant or specific trend of the surface charge of the different samples as a function of test solutions concentration. Both PluS samples exhibit zeta potential in the range -1 ÷ -5 mV ($p > 0.05$), which indicates lack of electrostatic stabilisation of the colloidal dispersion.

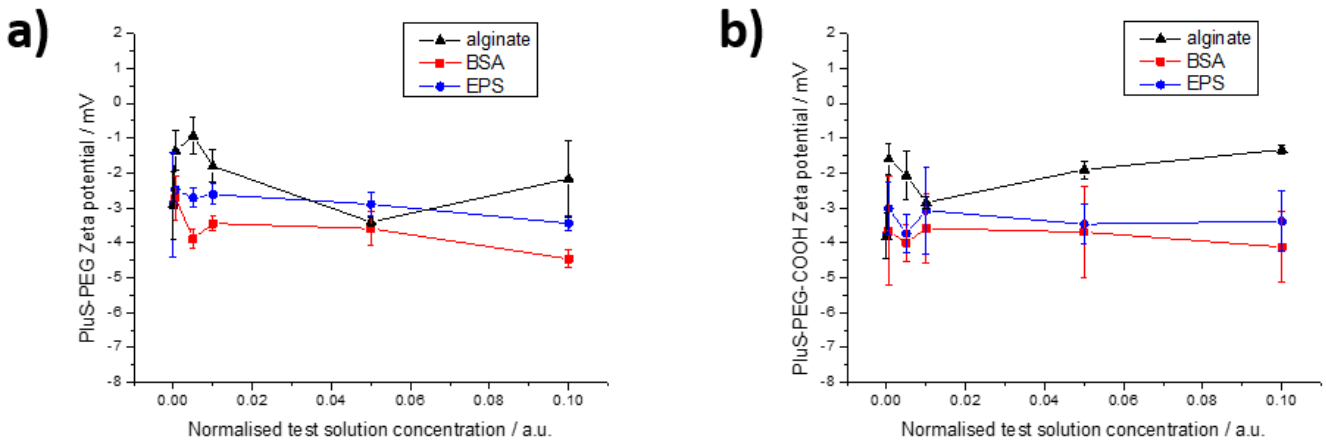

Figure 6. Zeta potential values measured for a) PluS-PEG and b) PluS-PEG-COOH dispersions exposed to *P. putida* EPS solutions. Error bars represent standard error of the mean (n = 5). Statistical differences were assessed by one-way ANOVA ($p < 0.05$).

In the case of PluS-PEG-COOH, the substantially constant particles size at all concentrations of both EPS extract and alginate solutions (Figure 5b)), suggests that a stabilising interaction could be happening between the particles and the polysaccharides present in the EPS extract. Instead, the small size increment seen for NP-BSA samples suggests that the protein interacts with the particles, likely forming a protein corona promoted by the interaction with the carboxylic groups present on the nanoparticle surface.[38] Such preferential interaction is consistent with the preferential binding pattern

shown on confocal images (

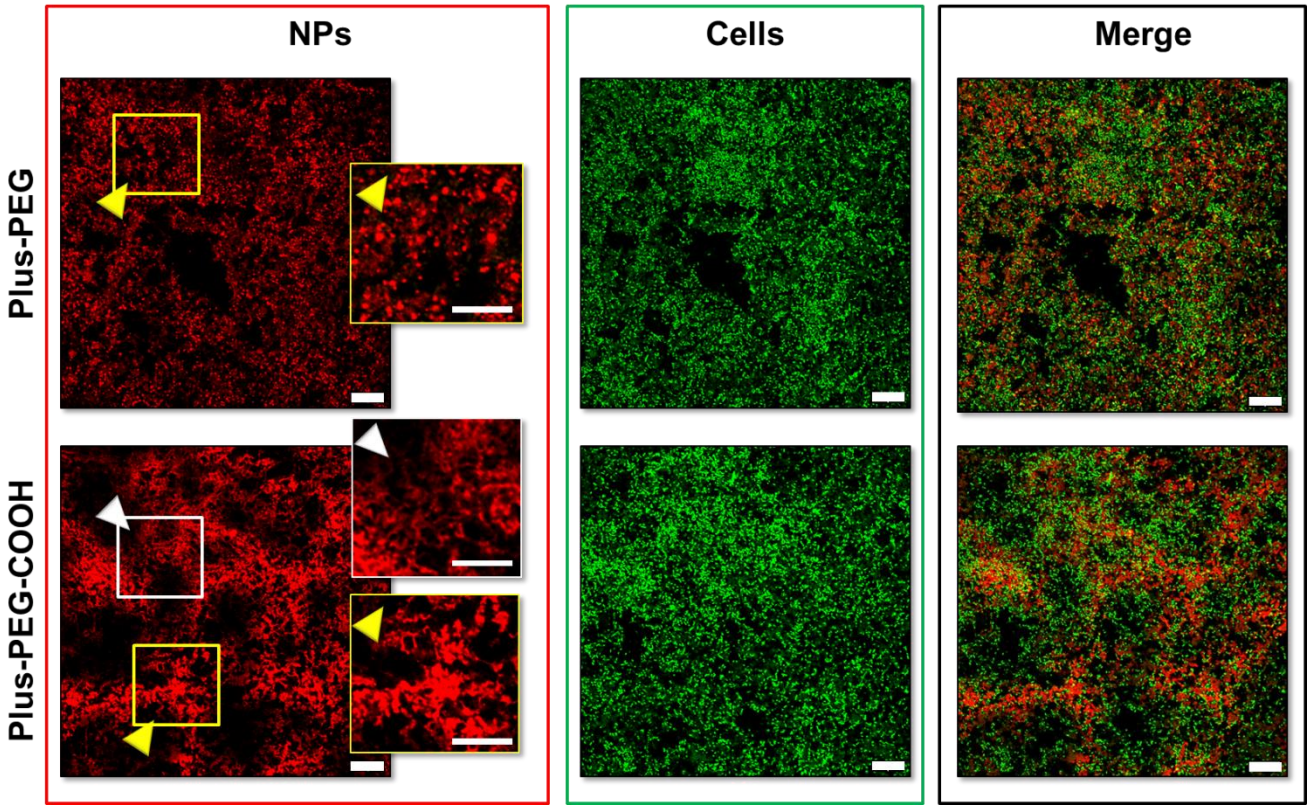

Figure ***4***) and with the colocalisation analysis data (Table 3).

For PluS-PEG, instead, the increase in hydrodynamic ratio exhibited in all the test solutions (Figure 5a)) indicates aggregation of the particle dispersions in all the conditions analysed. This decrease in colloidal stability in buffered and biomolecules solution is not commonly observed for NPs surrounded by a PEG shell (or PEGylated); on the contrary, the presence of a coating of PEG on the particle is usually associated with a stabilising effect caused by the minimisation of non-specific interactions and proteins adsorption, referred to as "stealth effect".[39] The stealth effect has been extensively investigated in the nanomedicine field and presents particle PEGylation as an effective strategy to increase bioavailability and circulation time of drugs and nanoparticle-based treatments in the bloodstream.[40] Although their antifouling properties are well documented, it is also understood that the extent of suppression of protein adsorption on PEGylated particles is affected by a number of factors, including polymer molecular weight, density and nanoparticle core material.[41] Furthermore, the polymeric chain conformation (e.g. brush or mushroom) can vary according to solvent and ionic strength of the medium, thus changing the surface structure and consequently its

affinity for proteins.[41a, 42] In addition, specific functional groups on the PEG shell or on the particle core can cause interaction with certain proteins to selectively occur. For these reasons, comparisons with literature data can be questionable, and a case-by-case analysis of the interactions involved might be needed.

However in our case, given that stable and non-buffered aqueous particle solutions were inoculated to the biofilms, it is reasonable to hypothesise that the agglomeration occurs after the particles enter the biofilm biomolecule-rich matrix.[43] If the formation of large aggregates occurred upon contact between the particles and the biofilm outer surface, the particles would rather accumulate on the surface itself instead of diffusing into the biofilm. Furthermore, for the formation of micrometric aggregates within the biofilm to occur a relatively large amount of captured particles would be required, and this is consistent with the higher particle entrapment (Figure 2) measured for PluS-PEG (25%) compared to PluS-PEG-COOH (12%). Furthermore, DLS size analysis carried out on 200 nM NPs dispersions in 0.9% NaCl (Table S1) shows no significant increase in dH (in spite of the lack of electrostatic stabilisation, demonstrated by the decrease in zeta potential); this is proof of PluS particles stability in the physiological environment simulated in the experiments, and ensures that any aggregation or stabilisation process observed would derive from the NP-biomolecules interaction only.

The PluS-PEG particles are able to penetrate and diffuse inside the biofilm matrix and they were not observed to show strong affinity to specific biofilm components, but medium colocalisation to both polysaccharides and proteins (Table 3). This behaviour in the biofilm is consistent with data reported on the diffusion of PEGylated polystyrene NPs inside *P. aeruginosa* and *B. multivorans* biofilms;[44] from the data reported it was concluded that PEGylated particles were able to freely diffuse within the biofilm without specifically binding to any components (matrix or cells). Free diffusive transport was also modelled for PEGylated L-tyrosine polyphosphate in *P. aeruginosa* biofilms, with experimental data supporting the theoretical model.[45] In spite of the strong aggregation occurring for PluS-PEG dispersions in EPS, BSA and alginate solution, the behaviour of the particles within the

biofilm can be associated with a stealth-like behaviour, which minimises non-specific interactions and results in uniform lateral distribution and axial diffusion along the biofilm thickness.[39]

These features have significant implications in the context of biofilm technology, where increased antibacterial and antibiofilm performances have been reported for PEGylated drug-nanocarriers, associated with an improved diffusion and penetration in the biofilm given by the PEG-shell.[46] It must be pointed out, however, that other studies report instead that certain PEG-functionalised particles are not able to effectively penetrate the biofilms,[47] unless the PEG-shell is combined with another functional group that can interact and bind to the matrix.[26c, 48]

To fully understand why some particles perform better than others it is important to consider that specific EPS matrix composition and characteristics – such as architecture, density, actual pore size, and viscosity – are key to selective interactions;[5b] furthermore, given that the EPS composition is quite heterogeneous in terms of proteins and polysaccharides, it cannot be excluded that competitive adsorption equilibria take place between the bio(macro)molecules on the particle surface and can lead to preferential binding of specific families of molecules.[49] Therefore, attention must be paid in generalisation, as a comprehensive model of the biofilm-nanoparticle interaction is likely described by a combination of several specific interactions, and understanding which interaction is more predominant is not a trivial task.

Overall, the results of the stability experiments in solution for both particles support those of confocal imaging and entrapment measurements, and in summary indicate that the different surface chemistry of the particle plays a major role in their transport and distribution within the biofilm. In our case, the aggregation observed for PluS-PEG in EPS matrix solutions could be symptomatic of non-specific interactions (likely steric or polymer bridging-like) occurring between the particle and multiple components of the matrix, and which prompt the particle entrapment and a uniform accumulation within the biofilm with no preferential localisation. For PluS-PEG-COOH the slight increase in size of the particles shown in BSA solutions only, coupled with the high colocalisation to proteins in the

biofilms, suggests that preferential interaction with proteins might drive the entrapment and subsequent accumulation of the particles in specific regions of the biofilm.

CONCLUSIONS

This study shows that PluS particles are, in general, captured effectively by *P. putida* biofilms and are transported through the entire biofilm depth. The different particle surface chemistry is associated to the different lateral distribution and specific affinity to matrix components that the two sets of PluS particles show. Effective transport through the biofilm coupled with specific lateral distribution are very relevant features in the context of the prospective application of the particles for development of antibiofilm technology. The higher entrapment with lower specific affinity makes PluS-PEG particles more applicable for non-targeted applications in antibiofilm technology: a high amount of particles captured coupled with unhindered diffusion throughout the entire biofilm and the bacterial microcolonies are required for using the particles, for example, as carriers of non-specific matrix dispersing agents or antibiotic agents. On the other hand, Plus-PEG-COOH are more promising for applications where matrix protein-targeting is desired. Follow up studies will involve the design of PluS particles engineered with functional systems (e.g. antimicrobial agents, enzymes for matrix dispersion, biomolecules to target biofilm physiological processes, dyes for phototermal therapy), to develop smart nanomaterials for biofilm control.

This work supports the rational design of functional NPs as a platform for the development of NP-based anti-biofilm technology that will overcome the challenges associated with the EPS matrix.

ASSOCIATED CONTENT

Supporting Information

Representative TEM images and hydrodynamic diameter distributions of PluS-PEG and PluS-PEG-COOH NPs, high-magnification CLSM images of bacterial biofilms after exposure to PluS-PEG and PluS-PEG-COOH NPs and matrix components staining.

AUTHOR INFORMATION

Corresponding Authors

Stefania Vitale, UCD School of Chemical and Bioprocess Engineering, University College Dublin, Dublin 4, Ireland

† Present address: Université de Strasbourg, CNRS, ISIS, 8 allée Gaspard Monge, 67000 Strasbourg, France

Email : svitale@unistra.fr

Author Contributions

The manuscript was written through contributions of all authors. All authors have given approval to the final version of the manuscript.

Funding sources

This research was supported by Science Foundation Ireland (SFI) under grant number 15/IA/3008.

Notes

The authors declare no competing financial interest.

ACKNOWLEDGMENT

This research was supported by Science Foundation Ireland (SFI) under Grant Number 15/IA/3008. The authors would like to thank Prof. Dr. Kenneth Dawson from Centre for BioNano Interactions (CBNI) UCD for the Zetasizer equipment.

REFERENCES

1. Stoodley, P.; Sauer, K.; Davies, D. G.; Costerton, J. W., Biofilms as complex differentiated communities. *Annual Review of Microbiology* **2002,** *56*, 187-209.
2. Starkey, M.; Parsek, M. R.; Gray, K. A.; Chang, S. I., A Sticky Business: the Extracellular Polymeric Substance Matrix of Bacterial Biofilms. In *Microbial Biofilms*, American Society of Microbiology: 2004.
3. Wang, L. L.; Hu, C.; Shao, L. Q., The antimicrobial activity of nanoparticles: present situation and prospects for the future. *International Journal of Nanomedicine* **2017,** *12*, 1227-1249.
4. (a) Berini, F.; Orlandi, V.; Gornati, R.; Bernardini, G.; Marinelli, F., Nanoantibiotics to fight multidrug resistant infections by Gram-positive bacteria: hope or reality? *Biotechnology Advances* **2022,** *57*, 107948; (b) Liu, Y.; Shi, L.; Su, L.; van der Mei, H. C.; Jutte, P. C.; Ren, Y.; Busscher, H. J., Nanotechnology-based antimicrobials and delivery systems for biofilm-infection control. *Chem. Soc. Rev.* **2019,** *48* (2), 428-446.
5. (a) Zanoni, M.; Habimana, O.; Amadio, J.; Casey, E., Antifouling activity of enzyme-functionalized silica nanobeads. *Biotechnology and Bioengineering* **2016,** *113* (3), 501-512; (b) Miller, K. P.; Wang, L.; Benicewicz, B. C.; Decho, A. W., Inorganic nanoparticles engineered to attack bacteria. *Chemical Society Reviews* **2015,** *44* (21), 7787-7807.
6. Pallavicini, P.; Dona, A.; Taglietti, A.; Minzioni, P.; Patrini, M.; Dacarro, G.; Chirico, G.; Sironi, L.; Bloise, N.; Visai, L.; Scarabelli, L., Self-assembled monolayers of gold nanostars: a convenient tool for near-IR photothermal biofilm eradication. *Chemical Communications* **2014,** *50* (16), 1969-1971.
7. Dunsing, V.; Irmscher, T.; Barbirz, S.; Chiantia, S., Purely Polysaccharide-Based Biofilm Matrix Provides Size-Selective Diffusion Barriers for Nanoparticles and Bacteriophages. *Biomacromolecules* **2019,** *20* (10), 3842-3854.
8. (a) Flemming, H. C., *The Biofilm Mode of Life*. Wiley-V C H Verlag Gmbh: Weinheim, 2015; p 279-291; (b) Sankaran, J.; Tan, N. J. H. J.; But, K. P.; Cohen, Y.; Rice, S. A.; Wohland, T., Single microcolony diffusion analysis in Pseudomonas aeruginosa biofilms. *npj Biofilms and Microbiomes* **2019,** *5* (1), 35; (c) González, S.; Fernández, L.; Gutiérrez, D.; Campelo, A. B.; Rodríguez, A.; García, P., Analysis of Different Parameters Affecting Diffusion, Propagation and Survival of Staphylophages in Bacterial Biofilms. *Frontiers in Microbiology* **2018,** *9*.
9. (a) Stewart, P. S., Diffusion in biofilms. *J Bacteriol* **2003,** *185* (5), 1485-1491; (b) van den Berg, L.; van Loosdrecht, M. C. M.; de Kreuk, M. K., How to measure diffusion coefficients in biofilms: A critical analysis. *Biotechnology and bioengineering* **2021,** *118* (3), 1273-1285.
10. (a) Ikuma, K.; Decho, A. W.; Lau, B. L. T., When nanoparticles meet biofilms-interactions guiding the environmental fate and accumulation of nanoparticles. *Frontiers in Microbiology* **2015,** *6*, 6; (b) Fulaz, S.; Vitale, S.; Quinn, L.; Casey, E., Nanoparticle–Biofilm Interactions: The Role of the EPS Matrix. *Trends in Microbiology* **2019**.
11. (a) Petrizza, L.; Collot, M.; Richert, L.; Mely, Y.; Prodi, L.; Klymchenko, A. S., Dye-doped silica nanoparticle probes for fluorescence lifetime imaging of reductive environments in living cells. *Rsc Advances* **2016,** *6* (106), 104164-104172; (b) Arca, M.; Caltagirone, C.; De Filippo, G.; Formica, M.; Fusi, V.; Giorgi, L.; Lippolis, V.; Prodi, L.; Rampazzo, E.; Scorciapino, M. A.; Sgarzi, M.; Zaccheroni, N., A fluorescent ratiometric nanosized system for the determination of Pd-II in water. *Chemical Communications* **2014,** *50* (96), 15259-15262; (c) Biffi, S.; Petrizza, L.; Garrovo, C.; Rampazzo, E.; Andolfi, L.; Giustetto, P.; Nikolov, I.; Kurdi, G.; Danailov, M. B.; Zauli, G.; Secchiero, P.; Prodi, L., Multimodal near-infrared-emitting PluS Silica nanoparticles with fluorescent, photoacoustic, and photothermal capabilities. *International Journal of Nanomedicine* **2016,** *11*, 4865-4874; (d) Soster, M.; Juris, R.; Bonacchi, S.; Genovese, D.; Montalti, M.; Rampazzo, E.; Zaccheroni, N.; Garagnani, P.; Bussolino, F.; Prodi, L.; Marchio, S., Targeted dual-color silica nanoparticles provide univocal identification of micrometastases in preclinical models of colorectal cancer. *International Journal of Nanomedicine* **2012,** *7*, 4797-4807; (e) Rampazzo, E.; Boschi, F.; Bonacchi, S.; Juris, R.; Montalti, M.; Zaccheroni, N.; Prodi, L.; Calderan, L.; Rossi, B.; Becchi, S.; Sbarbati, A., Multicolor core/shell silica nanoparticles for in vivo and ex vivo imaging. *Nanoscale* **2012,** *4* (3), 824-830; (f) Ambrosi, G.; Borgogelli, E.; Formica, M.; Fusi, V.; Giorgi, L.; Micheloni, M.; Rampazzo, E.; Sgarzi, M.; Zaccheroni, N.; Prodi, L., PluS

Nanoparticles as a tool to control the metal complex stoichiometry of a new thio-aza macrocyclic chemosensor for Ag(I) and Hg(II) in water. *Sensors and Actuators B-Chemical* **2015,** *207*, 1035-1044.
12. Peter, S.; Oberhettinger, P.; Schuele, L.; Dinkelacker, A.; Vogel, W.; Dorfel, D.; Bezdan, D.; Ossowski, S.; Marschal, M.; Liese, J.; Willmann, M., Genomic characterisation of clinical and environmental Pseudomonas putida group strains and determination of their role in the transfer of antimicrobial resistance genes to Pseudomonas aeruginosa. *Bmc Genomics* **2017,** *18*, 11.
13. (a) Chang, W. S.; van de Mortel, M.; Nielsen, L.; de Guzman, G. N.; Li, X. H.; Halverson, L. J., Alginate production by Pseudomonas putida creates a hydrated microenvironment and contributes to biofilm architecture and stress tolerance under water-limiting conditions. *Journal of Bacteriology* **2007,** *189* (22), 8290-8299; (b) Klausen, M.; Gjermansen, M.; Kreft, J. U.; Tolker-Nielsen, T., Dynamics of development and dispersal in sessile microbial communities: examples from Pseudomonas aeruginosa and Pseudomonas putida model biofilms. *Fems Microbiology Letters* **2006,** *261* (1), 1-11.
14. Santos, C.; Caetano, T.; Ferreira, S.; Mendo, S., Tn5090-like class 1 integron carrying bla(VIM-2) in a Pseudomonas putida strain from Portugal. *Clinical Microbiology and Infection* **2010,** *16* (10), 1558-1561.
15. Rampazzo, E.; Bonacchi, S.; Juris, R.; Montalti, M.; Genovese, D.; Zaccheroni, N.; Prodi, L.; Rambaldi, D. C.; Zattoni, A.; Reschiglian, P., Energy Transfer from Silica Core-Surfactant Shell Nanoparticles to Hosted Molecular Fluorophores. *Journal of Physical Chemistry B* **2010,** *114* (45), 14605-14613.
16. Helle, M.; Rampazzo, E.; Monchanin, M.; Marchal, F.; Guillemin, F.; Bonacchi, S.; Salis, F.; Prodi, L.; Bezdetnaya, L., Surface Chemistry Architecture of Silica Nanoparticles Determine the Efficiency of in Vivo Fluorescence Lymph Node Mapping. *Acs Nano* **2013,** *7* (10), 8645-8657.
17. Safari, A.; Habimana, O.; Allen, A.; Casey, E., The significance of calcium ions on Pseudomonas fluorescens biofilms - a structural and mechanical study. *Biofouling* **2014,** *30* (7), 859-69.
18. Devlin, H.; Hiebner, D.; Barros, C.; Fulaz, S.; Quinn, L.; Vitale, S.; Casey, E., A high throughput method to investigate nanoparticle entrapment efficiencies in biofilms. *Colloids and Surfaces B: Biointerfaces* **2020**, 111123.
19. Fulaz, S.; Hiebner, D.; Barros, C. H. N.; Devlin, H.; Vitale, S.; Quinn, L.; Casey, E., Ratiometric Imaging of the in Situ pH Distribution of Biofilms by Use of Fluorescent Mesoporous Silica Nanosensors. *ACS Applied Materials & Interfaces* **2019,** *11* (36), 32679-32688.
20. Schindelin, J.; Arganda-Carreras, I.; Frise, E.; Kaynig, V.; Longair, M.; Pietzsch, T.; Preibisch, S.; Rueden, C.; Saalfeld, S.; Schmid, B.; Tinevez, J.-Y.; White, D. J.; Hartenstein, V.; Eliceiri, K.; Tomancak, P.; Cardona, A., Fiji: an open-source platform for biological-image analysis. *Nat. Methods* **2012,** *9*, 676.
21. Bolte, S.; Cordelieres, F. P., A guided tour into subcellular colocalization analysis in light microscopy. *Journal of Microscopy-Oxford* **2006,** *224*, 213-232.
22. Jachlewski, S.; Jachlewski, W. D.; Linne, U.; Bräsen, C.; Wingender, J.; Siebers, B., Isolation of Extracellular Polymeric Substances from Biofilms of the Thermoacidophilic Archaeon Sulfolobus acidocaldarius. *Front Bioeng Biotechnol* **2015,** *3*, 123-123.
23. Bundschuh, M.; Filser, J.; Lüderwald, S.; McKee, M. S.; Metreveli, G.; Schaumann, G. E.; Schulz, R.; Wagner, S., Nanoparticles in the environment: where do we come from, where do we go to? *Environmental Sciences Europe* **2018,** *30* (1), 6.
24. Lim, J.; Yeap, S. P.; Che, H. X.; Low, S. C., Characterization of magnetic nanoparticle by dynamic light scattering. *Nanoscale Research Letters* **2013,** *8* (1), 381.
25. (a) Mi, G. J.; Shi, D.; Wang, M.; Webster, T. J., Reducing Bacterial Infections and Biofilm Formation Using Nanoparticles and Nanostructured Antibacterial Surfaces. *Advanced Healthcare Materials* **2018,** *7* (13), 23; (b) Canesi, L.; Corsi, I., Effects of nanomaterials on marine invertebrates. *Science of the Total Environment* **2016,** *565*, 933-940; (c) Joo, S. H.; Aggarwal, S., Factors impacting the interactions of engineered nanoparticles with bacterial cells and biofilms: Mechanistic insights and state of knowledge. *Journal of Environmental Management* **2018,** *225*, 62-74; (d) Rozenbaum, R. T.; Andrén, O. C. J.; van der Mei, H. C.; Woudstra, W.; Busscher, H. J.; Malkoch, M.; Sharma, P. K., Penetration and Accumulation of Dendrons with Different Peripheral Composition in Pseudomonas aeruginosa Biofilms. *Nano Letters* **2019,** *19* (7), 4327-4333.
26. (a) Ran, H. H.; Cheng, X. T.; Bao, Y. W.; Hua, X. W.; Gao, G.; Zhang, X. D.; Jiang, Y. W.; Zhu, Y. X.; Wu, F. G., Multifunctional quaternized carbon dots with enhanced biofilm penetration and eradication efficiencies. *Journal of Materials Chemistry B* **2019,** *7* (33), 5104-5114; (b) Duncan, B.; Li, X. N.; Landis, R. F.;

Kim, S. T.; Gupta, A.; Wang, L. S.; Ramanathan, R.; Tang, R.; Boerth, J. A.; Rotello, V. M., Nanoparticle-Stabilized Capsules for the Treatment of Bacterial Biofilms. *Acs Nano* **2015,** *9* (8), 7775-7782; (c) Liu, Y.; Busscher, H. J.; Zhao, B. R.; Li, Y. F.; Zhang, Z. K.; van der Mei, H. C.; Ren, Y. J.; Shi, L. Q., Surface-Adaptive, Antimicrobially Loaded, Micellar Nanocarriers with Enhanced Penetration and Killing Efficiency in Staphylococcal Biofilms. *Acs Nano* **2016,** *10* (4), 4779-4789; (d) Barros, C. H. N.; Hiebner, D. W.; Fulaz, S.; Vitale, S.; Quinn, L.; Casey, E., Synthesis and self-assembly of curcumin-modified amphiphilic polymeric micelles with antibacterial activity. *Journal of Nanobiotechnology* **2021,** *19* (1), 104.

27. Peulen, T. O.; Wilkinson, K. J., Diffusion of Nanoparticles in a Biofilm. *Environmental Science & Technology* **2011,** *45* (8), 3367-3373.

28. (a) Flemming, H. C.; Wingender, J., The biofilm matrix. *Nature Reviews Microbiology* **2010,** *8* (9), 623-633; (b) Flemming, H.-C.; Baveye, P.; Neu, T. R.; Stoodley, P.; Szewzyk, U.; Wingender, J.; Wuertz, S., Who put the film in biofilm? The migration of a term from wastewater engineering to medicine and beyond. *npj Biofilms and Microbiomes* **2021,** *7* (1), 10.

29. (a) Xiao, Y.; Wiesner, M. R., Transport and Retention of Selected Engineered Nanoparticles by Porous Media in the Presence of a Biofilm. *Environmental Science & Technology* **2013,** *47* (5), 2246-2253; (b) Miller, K. P.; Wang, L.; Chen, Y. P.; Pellechia, P. J.; Benicewicz, B. C.; Decho, A. W., Engineering nanoparticles to silence bacterial communication. *Frontiers in Microbiology* **2015,** *6*, 7.

30. Hiebner, D. W.; Barros, C.; Quinn, L.; Vitale, S.; Casey, E., Surface functionalization-dependent localization and affinity of SiO2 nanoparticles within the biofilm EPS matrix. *Biofilm* **2020,** *2*, 11.

31. Zinchuk, V.; Wu, Y.; Grossenbacher-Zinchuk, O., Bridging the gap between qualitative and quantitative colocalization results in fluorescence microscopy studies. *Sci. Rep.* **2013,** *3*, 1365.

32. Limoli, D. H.; Jones, C. J.; Wozniak, D. J., Bacterial Extracellular Polysaccharides in Biofilm Formation and Function. *Microbiology Spectrum* **2015,** *3* (3), 19.

33. (a) Walczyk, D.; Bombelli, F. B.; Monopoli, M. P.; Lynch, I.; Dawson, K. A., What the Cell "Sees" in Bionanoscience. *Journal of the American Chemical Society* **2010,** *132* (16), 5761-5768; (b) Ke, P. C.; Lin, S.; Parak, W. J.; Davis, T. P.; Caruso, F., A Decade of the Protein Corona. *Acs Nano* **2017,** *11* (12), 11773-11776; (c) Lundqvist, M.; Stigler, J.; Elia, G.; Lynch, I.; Cedervall, T.; Dawson, K. A., Nanoparticle size and surface properties determine the protein corona with possible implications for biological impacts. *Proceedings of the National Academy of Sciences of the United States of America* **2008,** *105* (38), 14265-14270.

34. Morrow, J. B.; Arango, C.; Holbrook, R. D., Association of Quantum Dot Nanoparticles with Pseudomonas aeruginosa Biofilm. *Journal of Environmental Quality* **2010,** *39* (6), 1934-1941.

35. (a) Hoshino, Y.; Lee, H.; Miura, Y., Interaction between synthetic particles and biomacromolecules: fundamental study of nonspecific interaction and design of nanoparticles that recognize target molecules. *Polymer Journal* **2014,** *46* (9), 537-545; (b) Meder, F.; Daberkow, T.; Treccani, L.; Wilhelm, M.; Schowalter, M.; Rosenauer, A.; Madler, L.; Rezwan, K., Protein adsorption on colloidal alumina particles functionalized with amino, carboxyl, sulfonate and phosphate groups. *Acta Biomaterialia* **2012,** *8* (3), 1221-1229.

36. (a) Adeleye, A. S.; Conway, J. R.; Perez, T.; Rutten, P.; Keller, A. A., Influence of Extracellular Polymeric Substances on the Long-Term Fate, Dissolution, and Speciation of Copper-Based Nanoparticles. *Environmental Science & Technology* **2014,** *48* (21), 12561-12568; (b) Mitzel, M. R.; Tufenkji, N., Transport of Industrial PVP-Stabilized Silver Nanoparticles in Saturated Quartz Sand Coated with Pseudomonas aeruginosa PAO1 Biofilm of Variable Age. *Environmental Science & Technology* **2014,** *48* (5), 2715-2723; (c) Barros, C. H. N.; Fulaz, S.; Vitale, S.; Casey, E.; Quinn, L., Interactions between functionalised silica nanoparticles and Pseudomonas fluorescens biofilm matrix: A focus on the protein corona. *Plos One* **2020,** *15* (7), 15.

37. Lebeaux, D.; Chauhan, A.; Rendueles, O.; Beloin, C., From in vitro to in vivo Models of Bacterial Biofilm-Related Infections. *Pathogens* **2013,** *2* (2), 288-356.

38. Brewer, S. H.; Glomm, W. R.; Johnson, M. C.; Knag, M. K.; Franzen, S., Probing BSA binding to citrate-coated gold nanoparticles and surfaces. *Langmuir* **2005,** *21* (20), 9303-9307.

39. Fam, S. Y.; Chee, C. F.; Yong, C. Y.; Ho, K. L.; Mariatulqabtiah, A. R.; Tan, W. S., Stealth Coating of Nanoparticles in Drug-Delivery Systems. *Nanomaterials (Basel)* **2020,** *10* (4).

40. (a) Li, D. Q.; Wang, F. C.; Di, H. X.; Liu, X. H.; Zhang, P. J.; Zhou, W.; Liu, D. B., Cross-Linked Poly(ethylene glycol) Shells for Nanoparticles: Enhanced Stealth Effect and Colloidal Stability. *Langmuir* **2019,** *35* (26), 8799-8805; (b) Gref, R.; Luck, M.; Quellec, P.; Marchand, M.; Dellacherie, E.; Harnisch, S.; Blunk, T.;

Muller, R. H., 'Stealth' corona-core nanoparticles surface modified by polyethylene glycol (PEG): influences of the corona (PEG chain length and surface density) and of the core composition on phagocytic uptake and plasma protein adsorption. *Colloids and Surfaces B-Biointerfaces* **2000,** *18* (3-4), 301-313; (c) Immordino, M. L.; Dosio, F.; Cattel, L., Stealth liposomes: review of the basic science, rationale, and clinical applications, existing and potential. *International Journal of Nanomedicine* **2006,** *1* (3), 297-315; (d) Klibanov, A. L.; Maruyama, K.; Torchilin, V. P.; Huang, L., AMPHIPATHIC POLYETHYLENEGLYCOLS EFFECTIVELY PROLONG THE CIRCULATION TIME OF LIPOSOMES. *Febs Letters* **1990,** *268* (1), 235-237; (e) Harris, J. M.; Chess, R. B., Effect of pegylation on pharmaceuticals. *Nature Reviews Drug Discovery* **2003,** *2* (3), 214-221.

41. (a) Jokerst, J. V.; Lobovkina, T.; Zare, R. N.; Gambhir, S. S., Nanoparticle PEGylation for imaging and therapy. *Nanomedicine* **2011,** *6* (4), 715-728; (b) Walkey, C. D.; Olsen, J. B.; Guo, H. B.; Emili, A.; Chan, W. C. W., Nanoparticle Size and Surface Chemistry Determine Serum Protein Adsorption and Macrophage Uptake. *Journal of the American Chemical Society* **2012,** *134* (4), 2139-2147.

42. Szleifer, I., Protein adsorption on surfaces with grafted polymers: A theoretical approach. *Biophysical Journal* **1997,** *72* (2), 595-612.

43. Choi, O. Y.; Yu, C. P.; Fernandez, G. E.; Hu, Z. Q., Interactions of nanosilver with Escherichia coli cells in planktonic and biofilm cultures. *Water Research* **2010,** *44* (20), 6095-6103.

44. Forier, K.; Messiaen, A. S.; Raemdonck, K.; Deschout, H.; Rejman, J.; De Baets, F.; Nelis, H.; De Smedt, S. C.; Demeester, J.; Coenye, T.; Braeckmans, K., Transport of nanoparticles in cystic fibrosis sputum and bacterial biofilms by single-particle tracking microscopy. *Nanomedicine* **2013,** *8* (6), 935-949.

45. Miller, J. K.; Neubig, R.; Clemons, C. B.; Kreider, K. L.; Wilber, J. P.; Young, G. W.; Ditto, A. J.; Yun, Y. H.; Milsted, A.; Badawy, H. T.; Panzner, M. J.; Youngs, W. J.; Cannon, C. L., Nanoparticle Deposition onto Biofilms. *Annals of Biomedical Engineering* **2013,** *41* (1), 53-67.

46. (a) Albayaty, Y. N.; Thomas, N.; Jambhrunkar, M.; Al-Hawwas, M.; Kral, A.; Thorn, C. R.; Prestidge, C. A., Enzyme responsive copolymer micelles enhance the anti-biofilm efficacy of the antiseptic chlorhexidine. *International Journal of Pharmaceutics* **2019,** *566*, 329-341; (b) Deepika, M. S.; Thangam, R.; Sundarraj, S.; Sheena, T. S.; Sivasubramanian, S.; Kulandaivel, J.; Thirumurugan, R., Co-delivery of Diverse Therapeutic Compounds Using PEG–PLGA Nanoparticle Cargo against Drug-Resistant Bacteria: An Improved Anti-biofilm Strategy. *ACS Applied Bio Materials* **2020,** *3* (1), 385-399.

47. Li, X. N.; Yeh, Y. C.; Giri, K.; Mout, R.; Landis, R. F.; Prakash, Y. S.; Rotello, V. M., Control of nanoparticle penetration into biofilms through surface design. *Chemical Communications* **2015,** *51* (2), 282-285.

48. Su, Y. L.; Zhao, L. L.; Meng, F. C.; Qiao, Z. Z.; Yao, Y.; Luo, J. B., Triclosan loaded polyurethane micelles with pH and lipase sensitive properties for antibacterial applications and treatment of biofilms. *Materials Science & Engineering C-Materials for Biological Applications* **2018,** *93*, 921-930.

49. (a) Lundqvist, M.; Stigler, J.; Cedervall, T.; Berggard, T.; Flanagan, M. B.; Lynch, I.; Elia, G.; Dawson, K., The Evolution of the Protein Corona around Nanoparticles: A Test Study. *Acs Nano* **2011,** *5* (9), 7503-7509; (b) Casals, E.; Pfaller, T.; Duschl, A.; Oostingh, G. J.; Puntes, V., Time Evolution of the Nanoparticle Protein Corona. *Acs Nano* **2010,** *4* (7), 3623-3632; (c) Stan, M. S.; Cinteza, L. O.; Petrescu, L.; Mernea, M. A.; Calborean, O.; Mihailescu, D. F.; Sima, C.; Dinischiotu, A., Dynamic analysis of the interactions between Si/SiO2 quantum dots and biomolecules for improving applications based on nano-bio interfaces. *Scientific Reports* **2018,** *8*, 11.